

'Failure Analysis of Thick Wire Bonds

by

Turker Dagdelen

A thesis
presented to the University of Waterloo
in fulfillment of the
thesis requirement for the degree of
Master of Applied Science
in
Mechanical Engineering

Waterloo, Ontario, Canada, 2013

©Turker Dagdelen 2013

AUTHOR'S DECLARATION

I hereby declare that I am the sole author of this thesis. This is a true copy of the thesis, including any required final revisions, as accepted by my examiners.

I understand that my thesis may be made electronically available to the public.

Abstract

In the last decade, reliability problems have become a critical subject in power modules. Understanding design weakness and failure mechanisms of thick wire bond are two critical steps in managing the risk of wire bond heel crack which is the topic of this thesis. Although this thesis does not target a specific type of power modules, we note that thick wire bond heel crack failures occur in Insulated Gate Bipolar Transistors (IGBTs). In fact, our aim is to understand failure mechanism in 300 μ m thick wire bonds with different geometries and materials. Since these wires experience harsh environmental conditions and high load transients, the wires undergo repetitive flexural movement which causes heel crack due to fatigue. For the purpose of understanding this failure mechanism, two experimental setups are built and utilized. The first experimental setup loads the wires using constant currents and observes the response using a scanning laser vibrometer to measure the displacement. The second experimental setup applies repetitive prescribed displacement to the first foot of the wire and detects fatigue failure using a Wheatstone bridge. It is realized that wires have different displacement property depending on their geometry and material. Maximum displacements are observed for Al-H11 instead of CuCorAl and PowerCu.

Acknowledgements

I would like to give my sincere thanks to Prof. Mustafa Yavuz and Prof. Eihab AbdelRahman for their support and supervision.

I am so thankful to Dr. Mahmoud and Dr. Sangtak for their endless help for this thesis and productive discussions. I thank Ahmed , Karim and Celal for their suggestions and useful feedbacks.

I would like thank Heraeus company and Steffen Koetter for their support.

I am thankful to my country for supporting me during Master.

Lastly, I am thankful to my lovely family.

Dedication

To my lovely family

Table of Contents

AUTHOR'S DECLARATION.....	ii
Abstract	iii
Acknowledgements.....	iv
Dedication	v
Table of Contents	vi
List of Figures	vii
List of Tables	ix
Chapter 1 Introduction and Literature Review	1
1.1 Wire Bonding and IGBT Modules.....	1
1.2 Reliability.....	6
1.2.1 Thermal cyclic test.....	8
1.2.2 Power Cyclic test	9
1.3 Mechanical cyclic test.....	10
Chapter 2 Specimen Preparation.....	11
Chapter 3 Joule Heating Experiment	19
3.1 Experimental Set-Up.....	20
3.2 Experiment Results	22
3.3 Simulation	25
3.4 Simulation Results	26
Chapter 4 Cyclic Vibration Test	30
4.1 Experimental Set Up	30
4.2 Mathematical Model	33
4.3 Experiment Results	38
Chapter 5 Conclusion	40
Conclusion	40
Bibliography.....	41

List of Figures

Figure 1.1. Packaging Levels [1].....	1
Figure 1.2. Wire Bond Production [2].....	2
Figure 1.3 Ball Bonding [3].....	2
Figure 1.4 Wedge Bonding [3].....	3
Figure 1.5 Wedge Bonding Process [3].....	3
Figure 1.6 Wire Material Chart [2].....	4
Figure 1.7 IGBT Module.....	5
Figure 1.8 Power Module Schematic [3].....	6
Figure 1.9 Wire Lift Off [7]	7
Figure 1.10 Heel Crack [10].....	8
Figure 1.11 Lift off (after test) [5].....	9
Figure 1.12 Lift off (side view) [5]	10
Figure 2.1 A-type of Substrate	11
Figure 2.2 B-type of Substrate.....	11
Figure 2.3 B-type substrates	12
Figure 2.4 A-type of substrates	13
Figure 2.5 Etching setup and SEM image of CuCorAl wire.....	15
Figure 2.6 PowerCu [13]	16
Figure 3.1 Wire bond (H: Height, L: Length)	19
Figure 3.2 Joule Heating Experimental Set-Up.....	20
Figure 3.3 Wire Bond Under Vibrometer.....	21
Figure 3.4 Current Displacement Relation.....	23
Figure 3.5 CuCorAl current- displacement relation	24
Figure 3.6 Temperature Sensor	26
Figure 3.7 Comsol Simulation.....	26
Figure 3.8 Vibrometer Result	27
Figure 3.9 Displacement distribution on wire	28
Figure 3.10 Temperature Distribution.....	28
Figure 4.1 Vibration Experimental Setup.....	31

Figure 4.2 Test Circuit	31
Figure 4.3 Test circuit schematic	32
Figure 4.4 Failure Detection	39
Figure 4.5 Heel Crack SEM Image.....	39

List of Tables

Table -1 Wire Dimensions and Materials	14
Table -2 Material Properties of Power-Cu and Al-H11	17
Table -3 Specimens	22
Table-4 Vibration test Results.....	38

Chapter 1

Introduction and Literature Review

1.1 Wire Bonding and IGBT Modules

Wire Bonding is the essential step of first-level electronics packaging. Basically, it makes electrical interconnection between integrated circuits and circuit board. Figure 1.1 [1] shows different electronic packaging steps, and wire bonding, typically, involves at the First level Packaging.

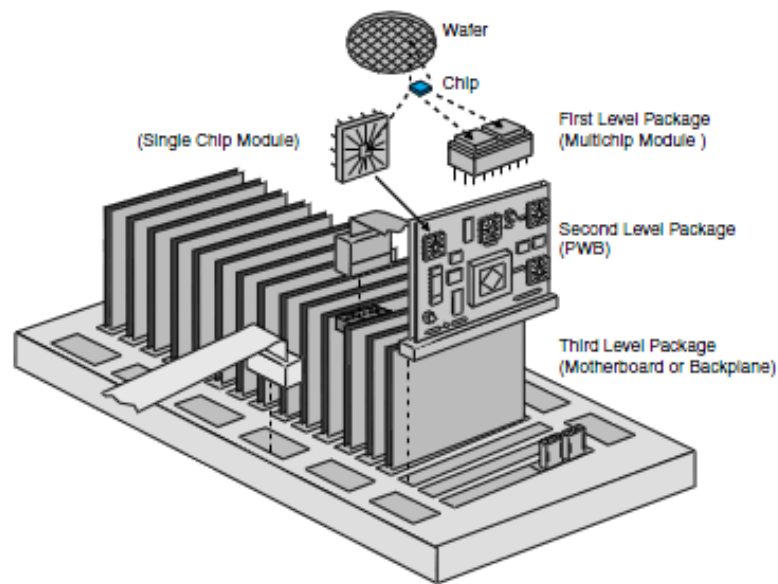


Figure 1.1. Packaging Levels [1]

It was calculated approximately in 1996 that 4×10^{12} wires were bonded per year [2] as indicated in Figure 1.2 [2].

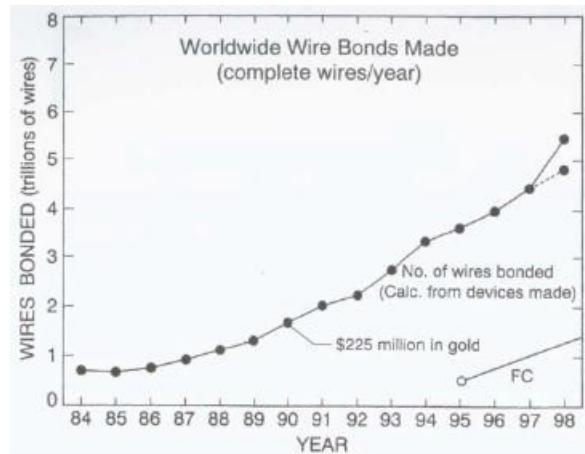


Figure 1.2. Wire Bond Production [2]

In this huge production, there are 2 main types of wire bonding; Wedge and Ball bonding, and these are in two forms as shown in Figure 1.3 and 1.4 [3] .

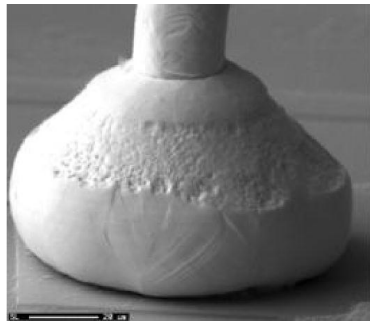


Figure 1.3 Ball Bonding [3]

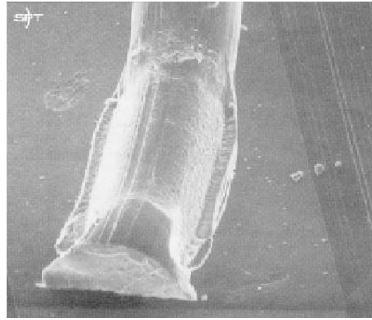


Figure 1.4 Wedge Bonding [3]

For both wedge and ball bonding, bonding step is achieved by wire bonders. As indicated in Figure 1.5 [3], machine tool makes several movements and applies ultrasonic forces to connect the wire on substrate. First and second feet of wires are achieved by these movements. Actually, this is one of the critical step that the heel part can be stressed and weakened during operation. Since initial stress is residual stress, wire life-time failure decreases with this operation.

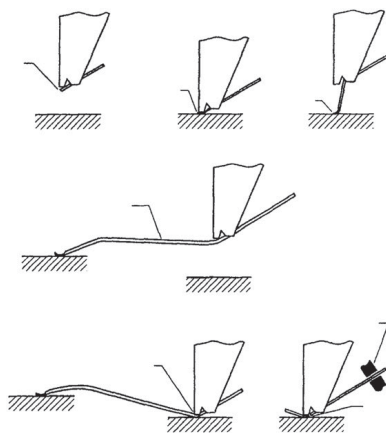


Figure 1.5 Wedge Bonding Process [3]

In terms of wire material, there are two types of it; Thin and Thick wires as shown in Fig. 1.6 [2].

Thin wires diameter is between 20-100 μm while thick wires are 100-500 μm . Thin wires are used in Micro Electro Mechanical Systems (MEMS). On the other hand, thick wires perform for power modulus due to their high current capacity.

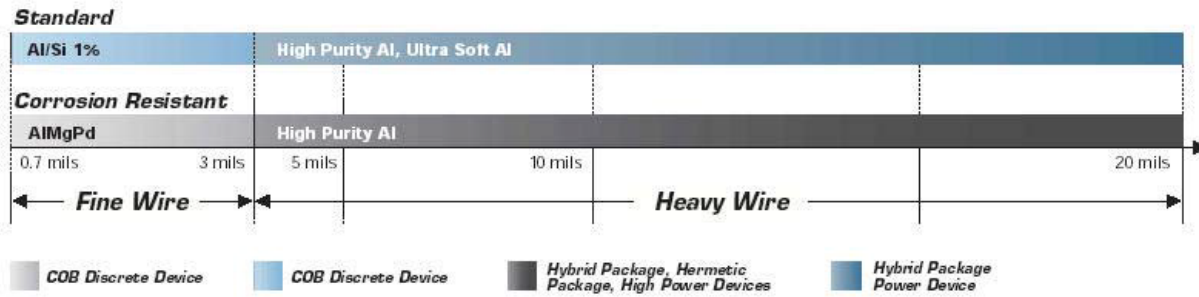


Figure 1.6 Wire Material Chart [2]

As mentioned before, thick wires are used in IGBT modulus. Figure 1.7 is a typical IGBT module with Aluminum (Al) wires. Depending up on current that is carried by thick wires, the number of wires can be reach 900.

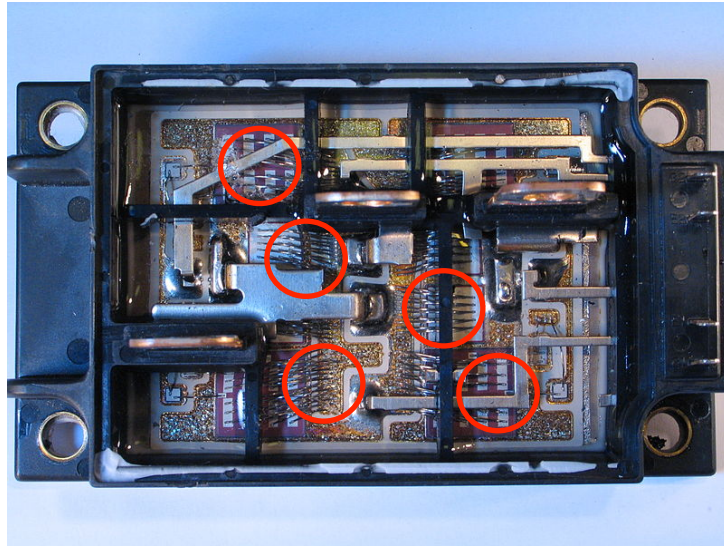


Figure 1.7 IGBT Module

1.2 Reliability

As indicated in Figure 1.8 [3], there are different types of failure mechanisms in power modulus depending up on transient and steady state conditions.

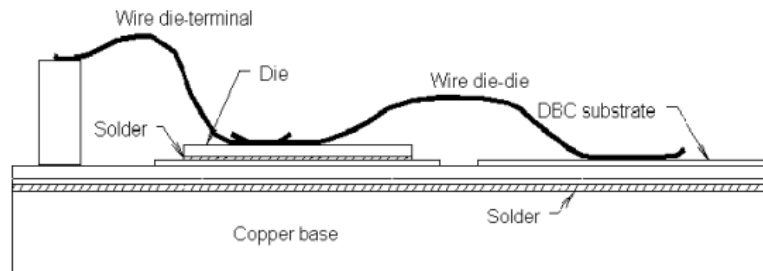


Figure 1.8 Power Module Schematic [3]

- Heel Crack Failure
- Wire failure near frame
- Bond failure near frame
- Wire lift off

These failures can be distinguished as; Sudden Failure (unpredictable) and Drift Failure (predictable and develop slowly) [10]. For example, one of them is extensively reported failure mechanism which is wire lift off [1, 3, 4, 5]. This failure occurs on the wire connection to chip surface due to chip metallization. Since cyclic heating and cooling

operations affect chip metallization, wire connections get weakened, and as a result it lifts off. It can be given as an example for Drift Failure.

Also, internal stress caused by different coefficient of thermal expansions (CTE) between wire material and substrate has an effect on it. Figure 1.9 [7] shows how lift off failure looks like.

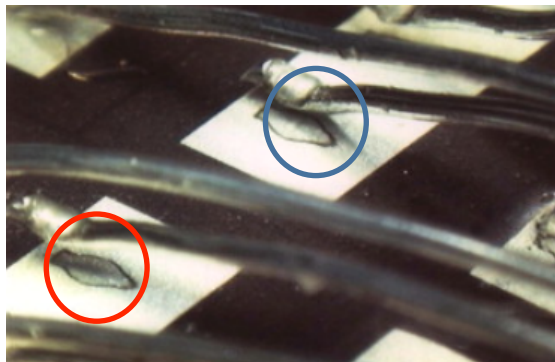


Figure 1.9 Wire Lift Off [7]

Beside, heel crack failure of ultrasonic wedge bond is also a challenging problem for a long time [2, 3, and 6.8]. Also, Lefranc [9] reports that one of the primary failure mechanisms of Insulated Gate Bipolar Transistors (IGBT) is wire bond failure. The risk of the crack due to the sharp wedge bonding tool, operator faults (for manual bonders), bonding machine itself vibration and rapid tool movement should be considered before wire serving life.

When wire starts to carry high currents and experiences harsh environmental conditions, number of failure mechanisms increase. Since all these failure mechanism and high temperature range between (-10) to (+150 °C) produce heel crack, and Figure 1.10 [8] shows an example of SEM image of the heel crack through the wire.

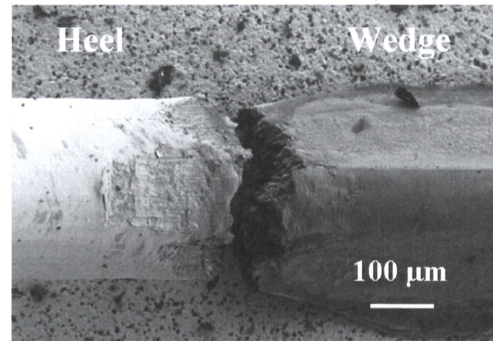


Figure 1.10 Heel Crack [10]

Failure of time can be estimated with different type of experiments; Temperature, Power and Vibration cyclic. Hence, experiment is an important step, so that components do not fail in unexpected times.

1.2.1 Thermal cyclic test

It is achieved by external heating and cooling systems. Thermal resistance at junction ($R_{th(jc)}$ [10]) is measured before and after test. If the results are not in the defined area, it means that test itself is not reliable. This is the decisive criterion for this test.

The junction temperature between chip and DCB (Direct Copper Bonded) is the focusing point of the test.

1.2.2 Power Cyclic test

Since module experiences heating by applying a load current, joule heating is the fundamental of this test mechanism. On the other hand , cooling is developed by turning of the power. Also, water cooling is used in these systems.

Even though thermal and power cyclic tests are almost same,the difference is cyclic times. Cyclic time in thermal test can reach minutes. On the other hand, in power cyclic test, it takes seconds [10].



Figure 1.11 Lift off (after test) [5]

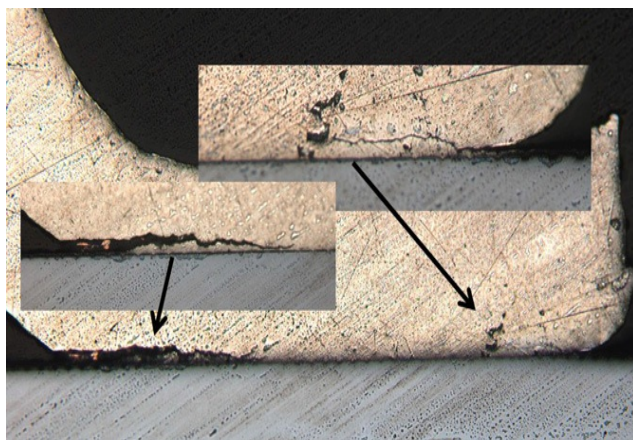


Figure 1.12 Lift off (side view) [5]

Figure 1.11 and 1.12 [5] shows lift off failure after power cyclic test. Crateria can be considered separation of wire from substrate.

1.3 Mechanical cyclic test

Vibration test is conducted for different purposes. Lefrance [9] performed a mechanical cyclic test for reliability assessments of wires after 1 billion cycles. This test mechanism is also performed to mimic lift off failure since traditional power-cycling tests are time-consuming.

Ramminger 's[6] vibration cyclic test was performed to analyze wire deformation under mechanical loadings (for separated bond surface applications). As a result, the relation between number of cycles to failure ad aspect ratio of wires (H/L) was explained. Same test mechanism was also extensively performed by Merkle [9] with different displacements and frequencies.

Chapter 2

Specimen Preparation

Since there are 2 types of experimental test setups, substrates are designed for different purposes. As shown in Figure 2.1, A-type of substrate is for Thermal test. On the other hand, Figure 2.2 shows B-type substrate which is for vibration test.

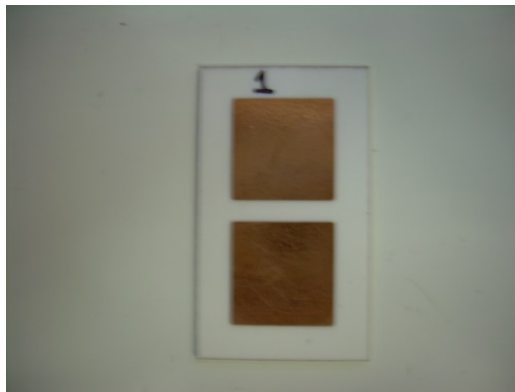


Figure 2.1 A-type of Substrate

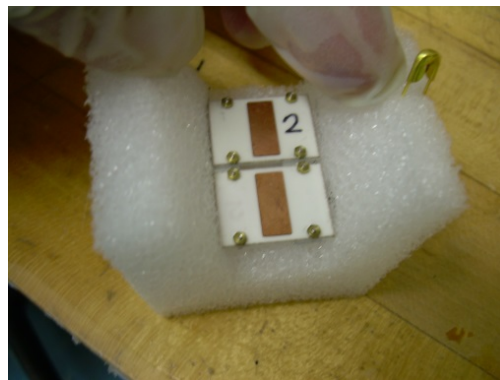


Figure 2.2 B-type of Substrate

These substrates are called Direct Copper Bonded (DCB). These types of substrates are used widely in power electronics. DCB substrates have two layers which are copper and ceramic. They fused together at high temperature and diffusion process. Copper is used for finish layer which is the wires are bonded on it. Three main ceramic types are that in use: Aluminum Oxide (Al_2O_3), Aluminum Nitride (AlN), and Silicon Nitride (Si_3N_4). These ceramics have low thermal resistance than other insulating materials. (Al_2O_3 : 24 W/mK and AlN : 130 W/mK). On the other hand, copper performs as a good heat spreading. Since copper substrate is cooled by baseplate, up to 3.6 kA can be handled with this substrate.

While A-type substrate has two separated copper surfaces, B-type substrate is connected externally. Since substrate is sent to Heraeus Company (Germany) for necessary wire connections, shipment safety becomes an important issue. To handle this problem, Styrofoams are designed for each substrate and packaged properly, as shown in Figure 2.3 and Figure 2.4.

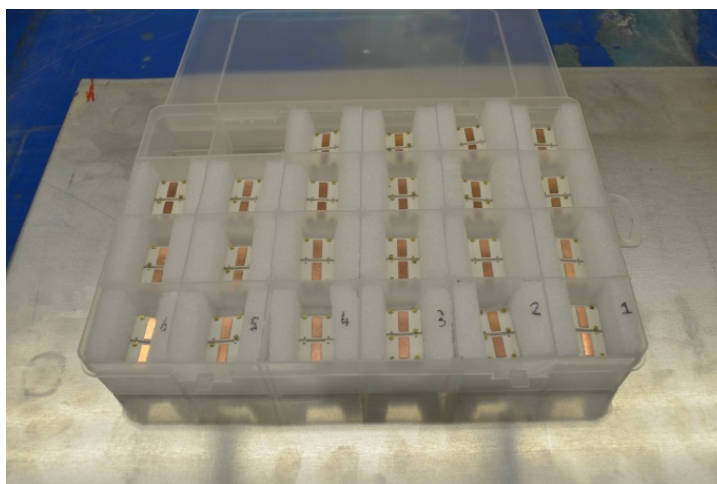


Figure 2.3 B-type substrates

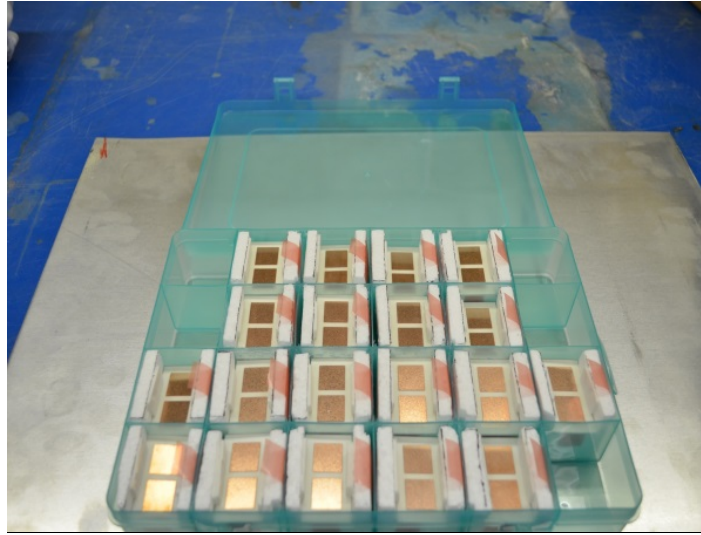


Figure 2.4 A-type of substrates

As shown in Table.1 ,different wires are bonded with different geometries

Sample Number (A type Substrate)	Material- Sample Number	Loop length(mm)	Loop Height(mm)
1-2	<i>Al-H11- 2 Samples</i>	9	3
3-4	<i>Al-H11- 2 S.</i>	9	3.5
5-6	<i>Al-H11- 2 S.</i>	9	4
7-8	Al-H11- 2 S.	10	3
9-10	Al-H11- 2 S.	10	3.5
11-12	Al-H11- 2 S.	10	4
13-14	Al-H11- 2 S.	11	3
15-16	Al-H11- 2 S.	11	3.5
17-18	Al-H11- 2 S.	11	4
19-20	CuCorAl- 2	9	3
21-22	CuCorAl- 2 S.	9	3.5
23-24	CuCorAl- 2 S.	9	4
25-26	CuCorAl- 2 S.	10	3
27-28	CuCorAl- 2 S.	10	3.5
29-30	CuCorAl- 2 S.	10	4
31-32	CuCorAl- 2 S.	11	3

33-34	CuCorAl- 2 S.	11	3.5
35-36	CuCorAl- 2 S.	11	4
37	PowerCu -1 Sample	9	*
38	PowerCu -1 S.	10	*
39-40	PowerCu -2 S.	11	*
Sample Number (B type Substrate)	Material- Sample Number	Loop length(mm)	Loop Height(mm)
1	Al-H11- 1 Sample	9	3
2-3	Al-H11- 1 S.	9	4
4	Al-H11- 1 S.	10	3
5-6	Al-H11- 1 S.	10	4
7	Al-H11- 1 S.	11	3
8-9	Al-H11- 1 S.	11	4
10	CuCorAl- 1 Samples	9	3
11-12	CuCorAl- 1 S.	9	4
13	CuCorAl- 1 S.	10	3
14-15	CuCorAl- 1 S.	10	4
16	CuCorAl- 1 S.	11	3
17-18	CuCorAl- 1 S.	11	4
19	PowerCu	11	*

Table-1 Wire Dimension and materials

- Al-H11 is 99.99% pure Al wire [9].

- CuCorAl wire is Al coated Cu wire. It has Cu core which is coated with Al. To be able to see Cu core, etching experiment is performed, and Scanning Electron Microscope (SEM) analysis is made, as shown in Figure 2.5.

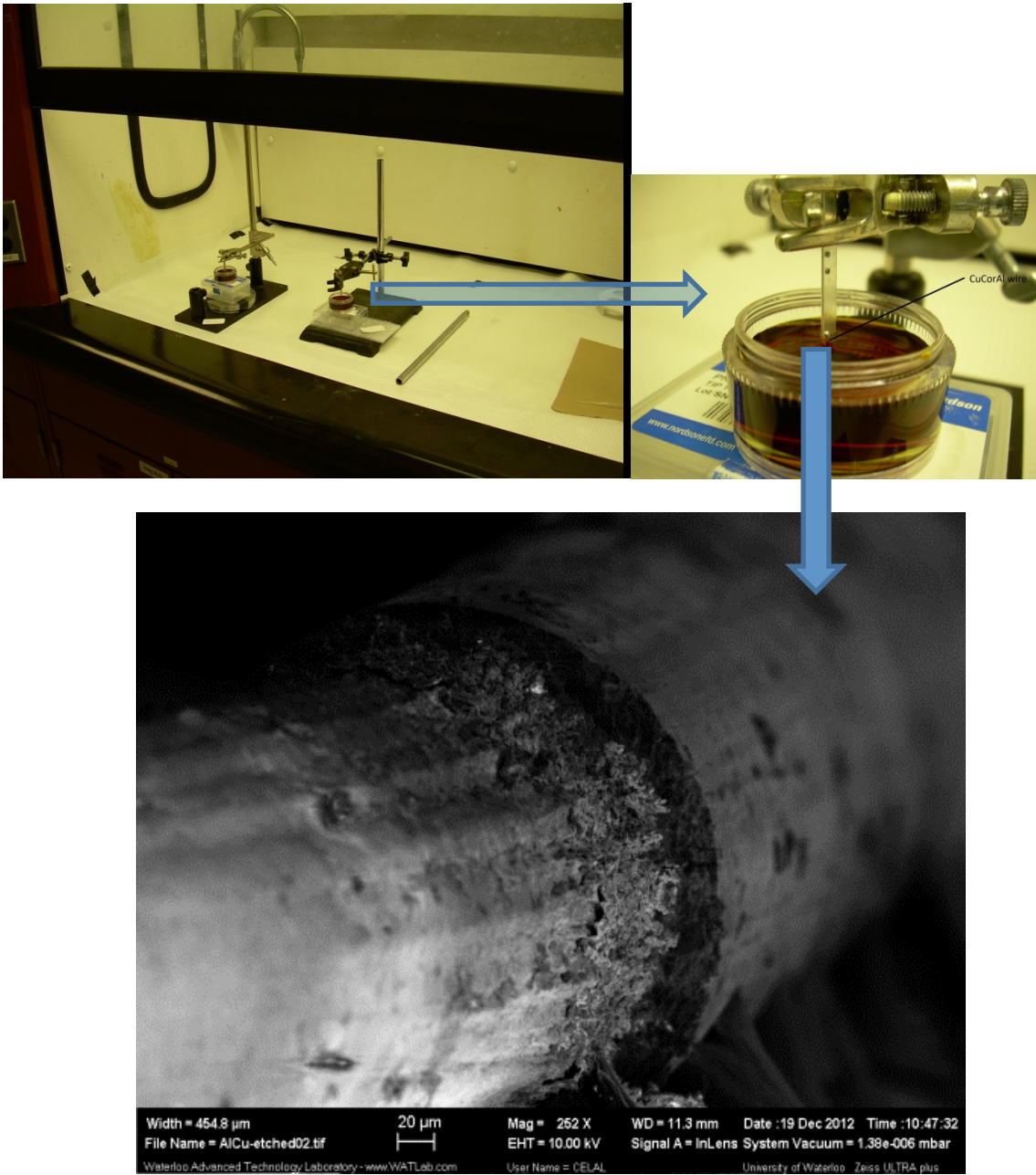


Figure 2.5 Etching setup and SEM image of CuCorAl wire

As shown in Figure 2.5, CuCorAl wire is etched with Ferric Chloride for 15-20 min. Then SEM image is taken. It seems clearly from the SEM image that Al layer is smaller than Copper core. Al layer thickness is around 25 μm , and Cu copper is about 250 μm .

PowerCu , as shown in Figure 2.6 [13], is pure Cu wire. Cu wires has been recently started to used for power modules. Since it is more conductive and can carry high current more than Al, it is preferred. Also, its cooling properties are better than Al.

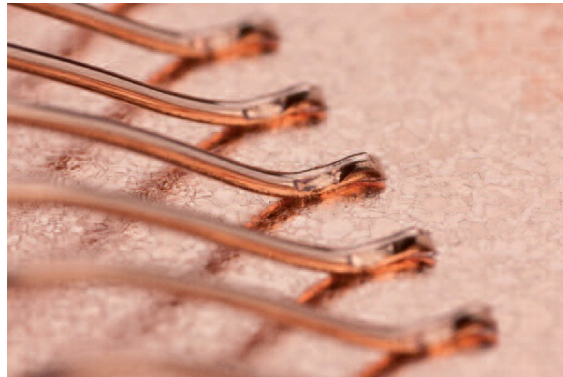


Figure 2.6 PowerCu [13]

Melting Point [°C]	1083	660
Modulus of rigidity [kN/mm ²]	48	27
Thermal conductivity at 20°C [W/m*K]	399	230
Linear expansion coefficient [10 ⁻⁶ *K ⁻¹]	16.8	25.3
Electrical Resistivity at 20°C [μW * cm]	1,8	2.8
Meter resistance at Ø 500 [μm mW/m]	(20°C) 91,7	(Ø 25 μm)57.1
Temperature coefficient of electrical resistance (0°C – 100°C) [10 ⁻³ * K ⁻¹]	3,9	4.14

Table-2 Material Properties of PowerCu and Al-H11 [13,14]

Table-2 [13, 14] gives comparison of properties of PowerCu and Al-H11 materials. As one can realize, Cu has less electrical resistivity which means better conductive than Al-H11. Also, thermal conductivity of PowerCu bigger than Al-H11, meaning it takes less time than Al-H11 time to cool down.

When an object experiences heating and cooling cycles, it expands which is determined by “Linear expansion coefficient” property. As can be seen from Table-2 , PowerCu makes less amount of expansion than Al-H11 for certain temperature.

Chapter 3

Joule Heating Experiment

Since thick wire bonds carry high currents, it causes displacement. Y direction shown in Figure 3.1, results in the maximum displacement compared to Z and X directions when it carries current [12]. In this sense, it means that wire heel max stress is determined by Y-Axis displacement.

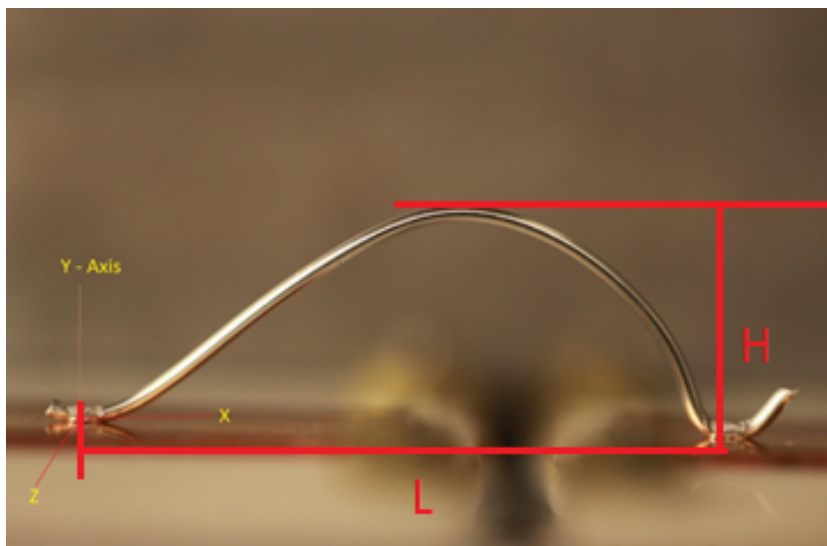


Figure 3.1 Wire bond (H: Height, L: Length)

Based on this information, we want to see how much displacement different wires make under constant currents conditions. This experimental setup reveals the ;

Displacement - Current,

- Wire loop,
- Material (Al-H11, CuCorAl, Cu) relations.

Additionally, Comsol- finite element method based- software is performed and compared with some experimental results.

3.1 Experimental Set-Up

As shown in Figure 3. 2, wires are excited by a Power Supply,with constant currents starting from 1A to 10 A.

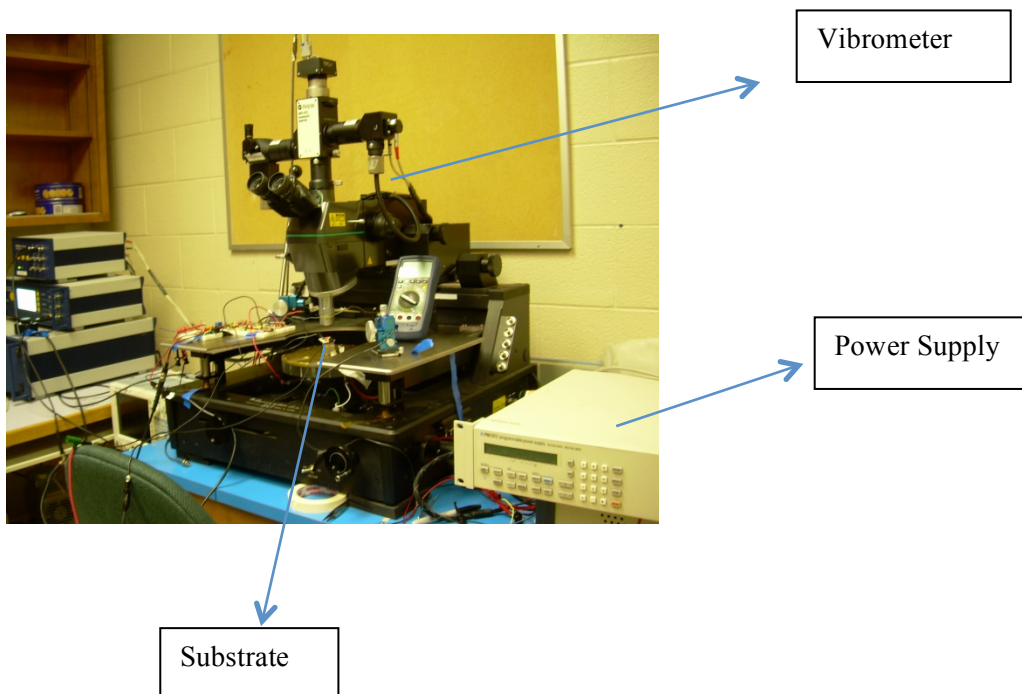


Figure 3.2 Joule Heating Experimental Set-Up

To be able to measure displacement on Y axis, laser-scanning vibrometer (Polytec MSV-400) is performed. The PSV-400 Vibrometer is a measurement tool for non-contact

measurement, and structural vibration analysis [15]. It can determine the operational deflection shape.

As shown in Figure 3.3, different wires (Table-3) are tested under vibrometer. White dot on the wire is laser beam which is in the middle of the wire.

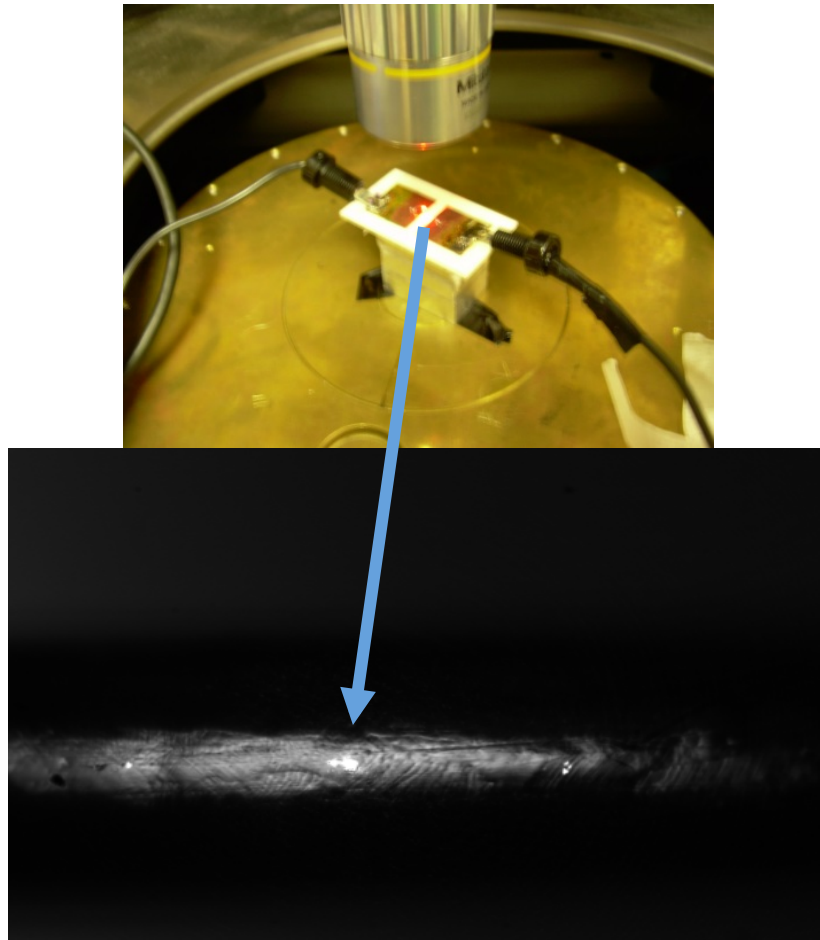


Figure 3.3 Wire Bond Under Vibrometer

It is noted that 10A maximum Direct Current (DC) value is safe since the fusion current for Al-H11 300 μm (\emptyset) wire is 15A.






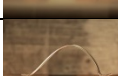

Sample Number (Al wire) (H/L)	Wire Image	Sample Number (CuCorAl wire) (H/L)	Wire Image
1 (3/9)		10 (3/9)	Identical to 1
2-3 (4/9)		11-12 (4/9)	Identical to 2
4 (3/10)		13 (3/10)	Identical to 4
5-6 (4/10)		14-15 (4/10)	Identical to 5
7 (3/11)		16 (3/11)	Identical to 7
8-9 (4/11)		17-18 (4/11)	Identical to 8
		19 (11/3)	

Table 3. Specimens

3.2 Experiment Results

As shown in Figure3. 4, Displacement – Current graph is plotted for different wires.

Aspect ratio (H/L) is the distinguished property.

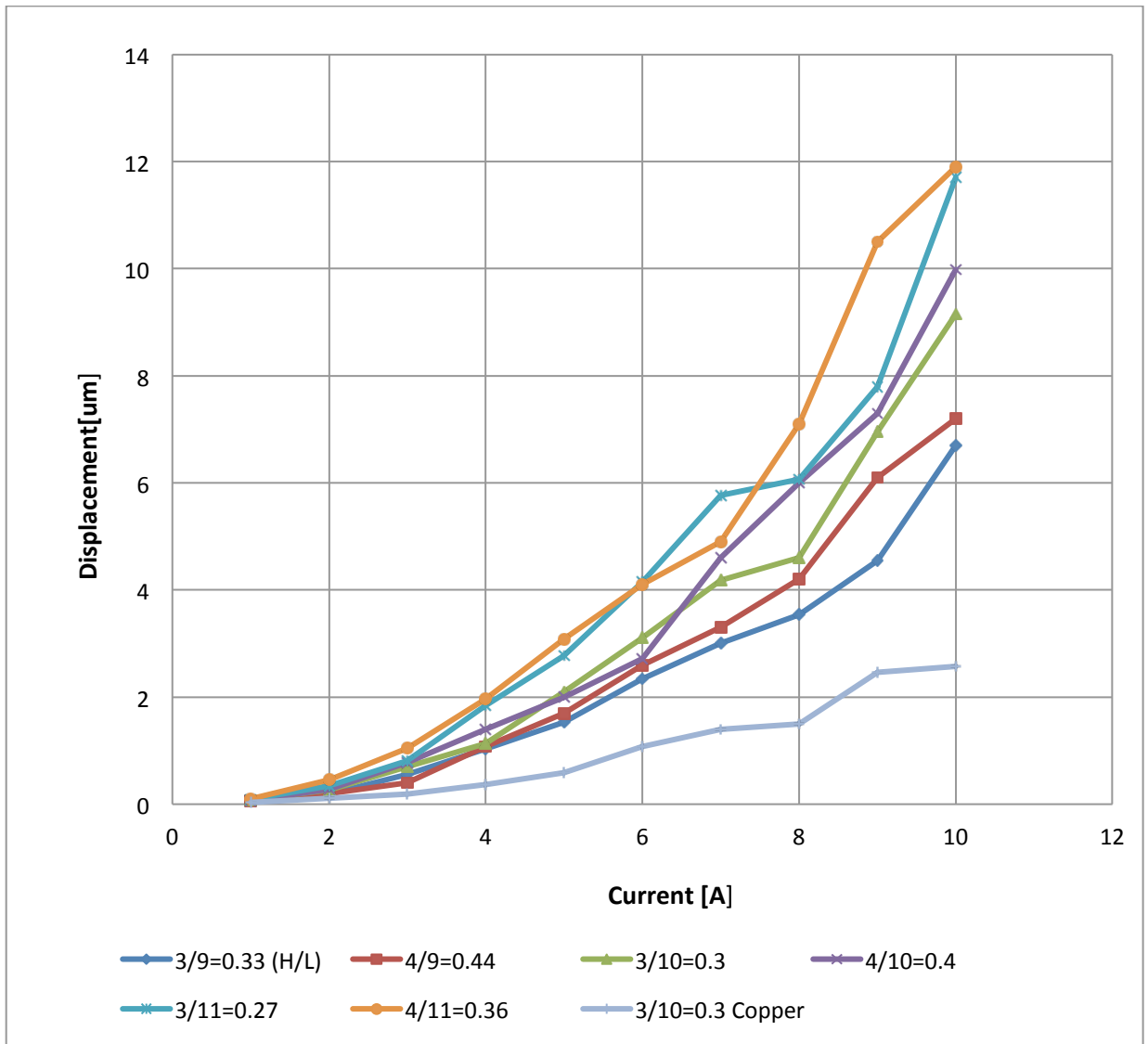


Figure 3.4 Current Displacement Relation

There are several conclusion can be made based on the results shown in Figure 3.4

- When the current increases, the displacement increases as well. This is expected since Joule heating is quadratically proportional to current. Likewise thermal stresses, and therefore peak wire displacement are proportional to heat generated in the wire.

- Measurements show that, when the length is the same for two wires, the higher one experiences more displacement.
- Measurements show that, when the height is the same for two wires, the longer one experiences more displacement
- The higher aspect ratio, the more wire displacement is realized.

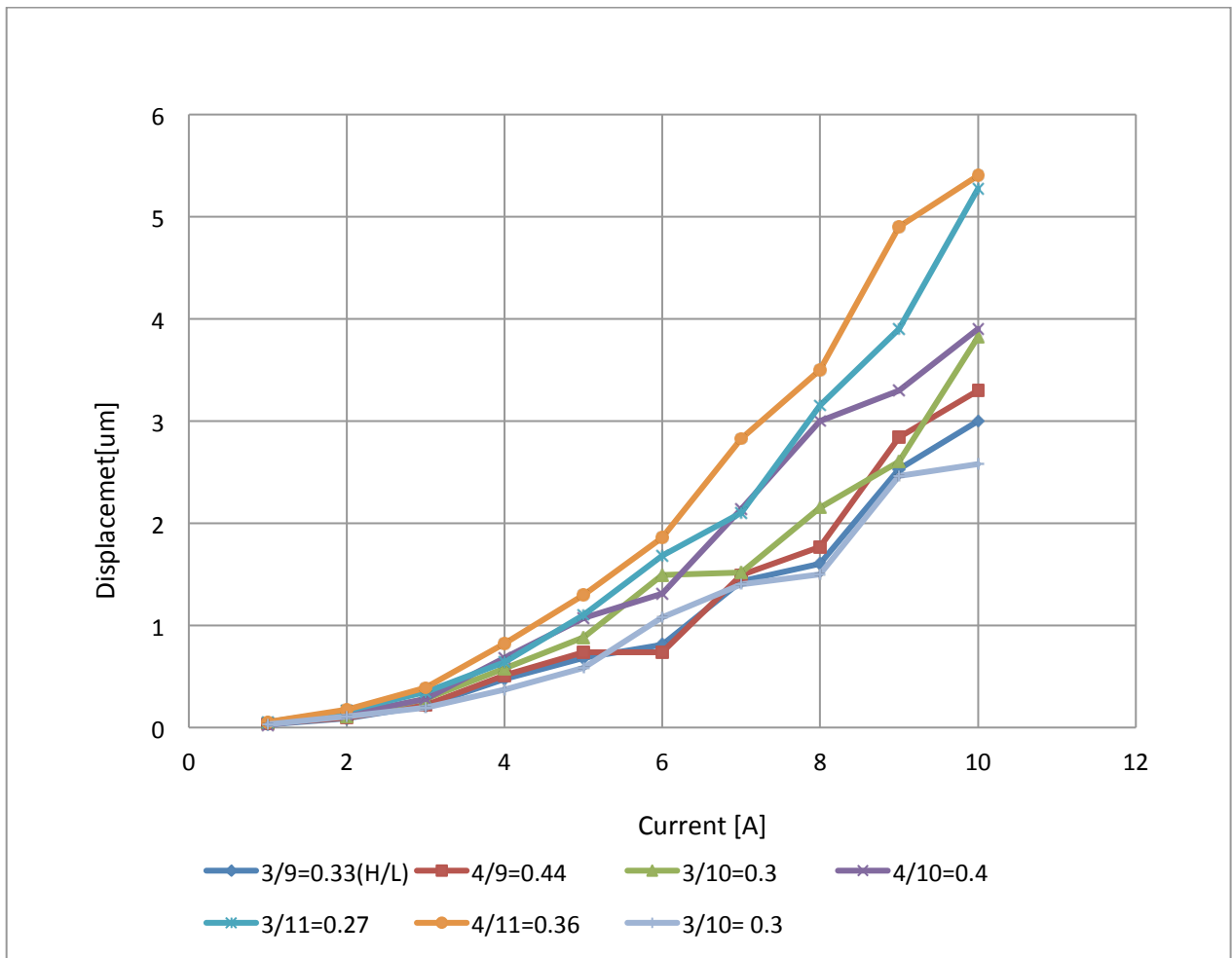


Figure 3.5 CuCorAl current- displacement relation

Al coated Copper (CuCorAl) current and displacement results are shown in Figure 3.5

3.3 Simulation

Wire is simulated by Comsol software. Since we would like to simulate wire in 3D and get the closest results to experimental values, SolidWorksLiveLink is used.

Simulation Steps:

- Wire is chosen as Al-H11 with 0.33 aspect ratio.
- 3D model is drawn by considering High Definition photo of wire and importing it in SolidWorks.
- 3D model is built identical to the wire.
- Then, Solidworks 3D file is imported in Comsol via SolidworksLiveLink (Synchronizing option)
- In Comsol , analyzing is made by “Joule Heating and Thermal Expansion (TEM)” module
- Since we make static analysis, boundary temperatures should be included considering the steady-state temperature. For this purpose, we use “Precision Centigrade Temperature Sensor-LM35” as shown in Figure3.6. Wire is excited by 10A, and substrate temperature is read as 26.85 °C at room temperature while 10 A constant current flows through wire. This value is imported in Comsol as a boundary condition (Junction Temperature).

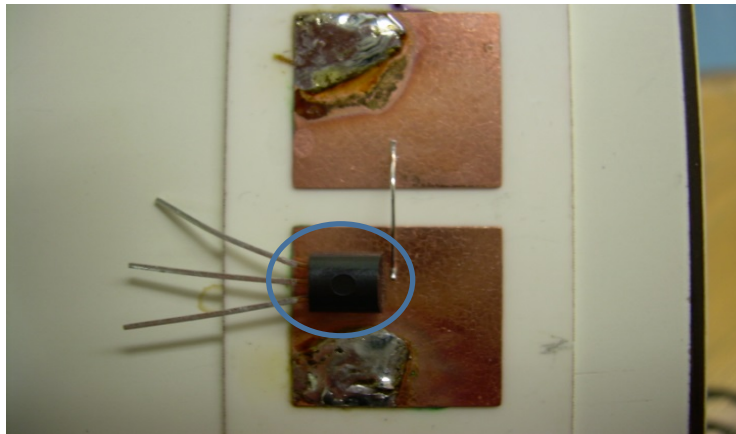


Figure 3.6 Temperature Sensor

3.4 Simulation Results

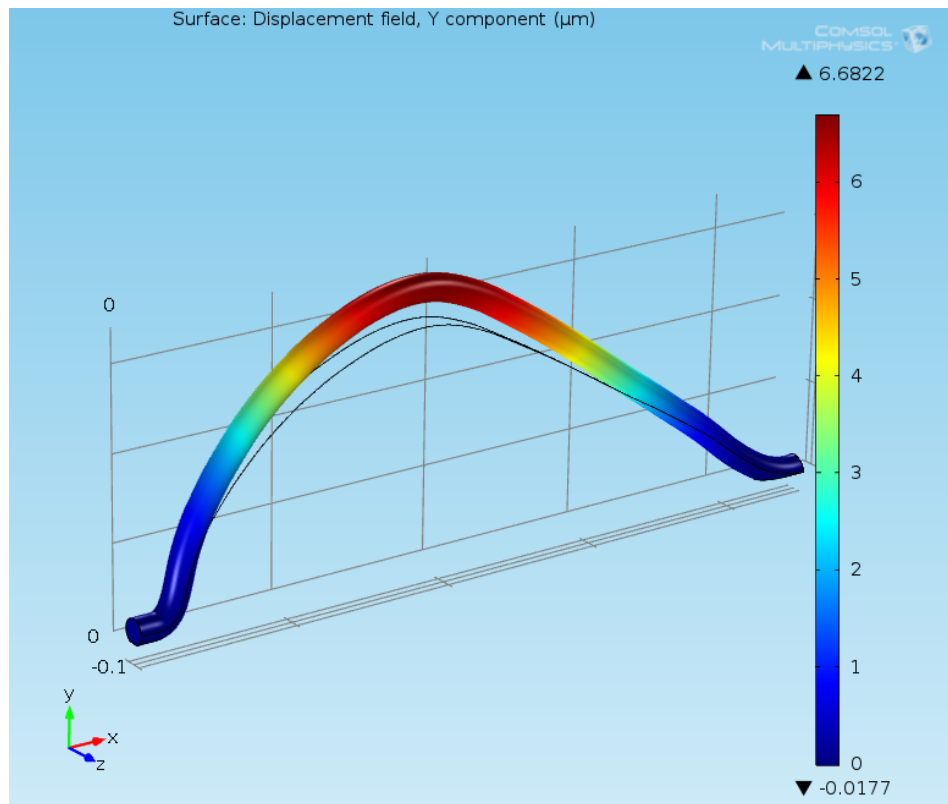


Figure 3.7 Comsol Simulation

As shown in Figure 3.7, wire displacement on Y-axis is $6.68 \mu\text{m}$. Experimental results for this wire, as shown in Figure 1.4, indicates that wire makes $6.7 \mu\text{m}$ displacements. As shown in Figure 3.8 , individual vibrometer analysis gives more clear displacement vision for this wire under 10A current.

By this way, our numerical model is validated.

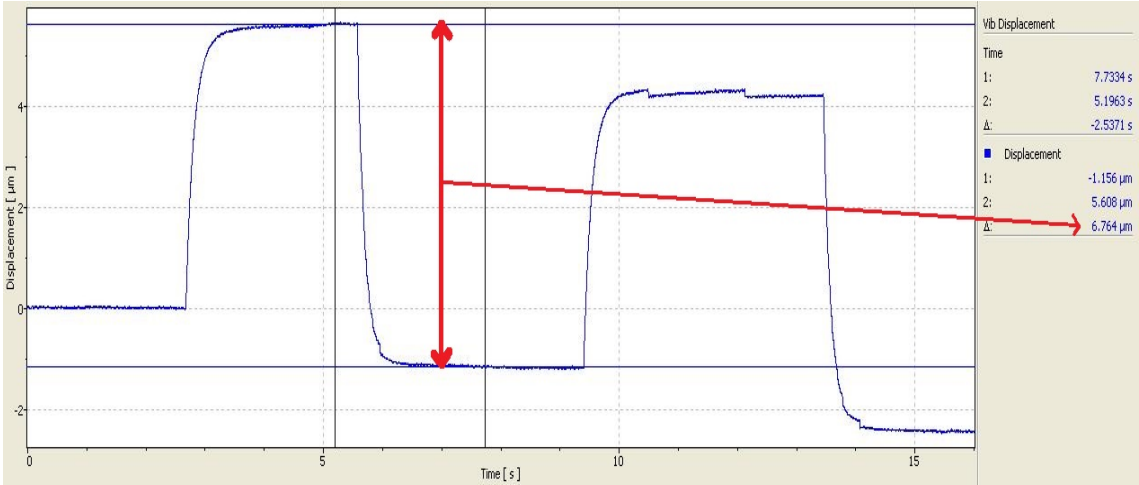


Figure 3.8 Vibrometer Result

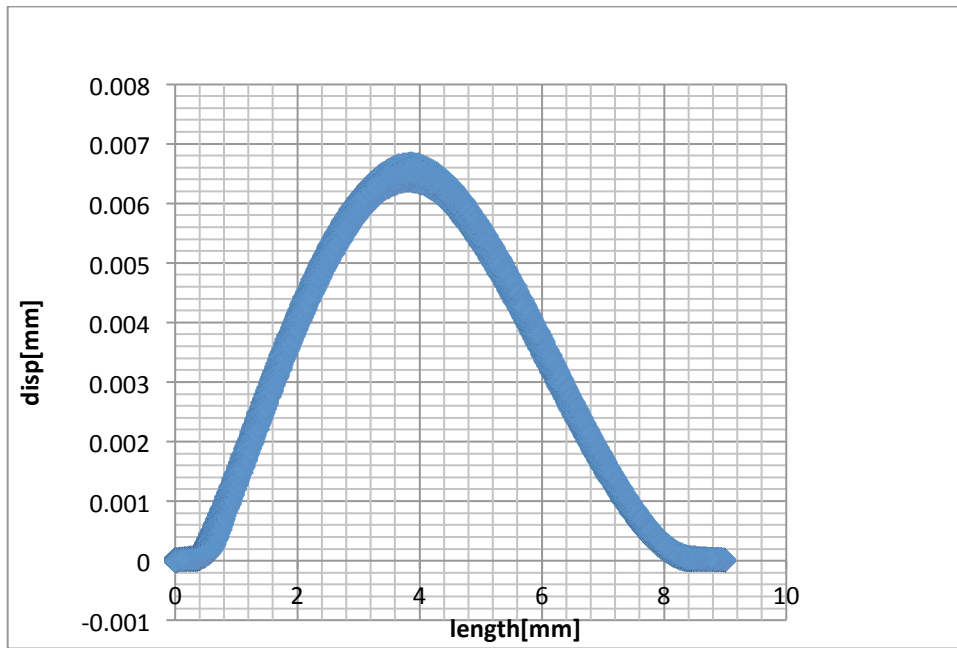


Figure 3.9 Displacement distribution on wire

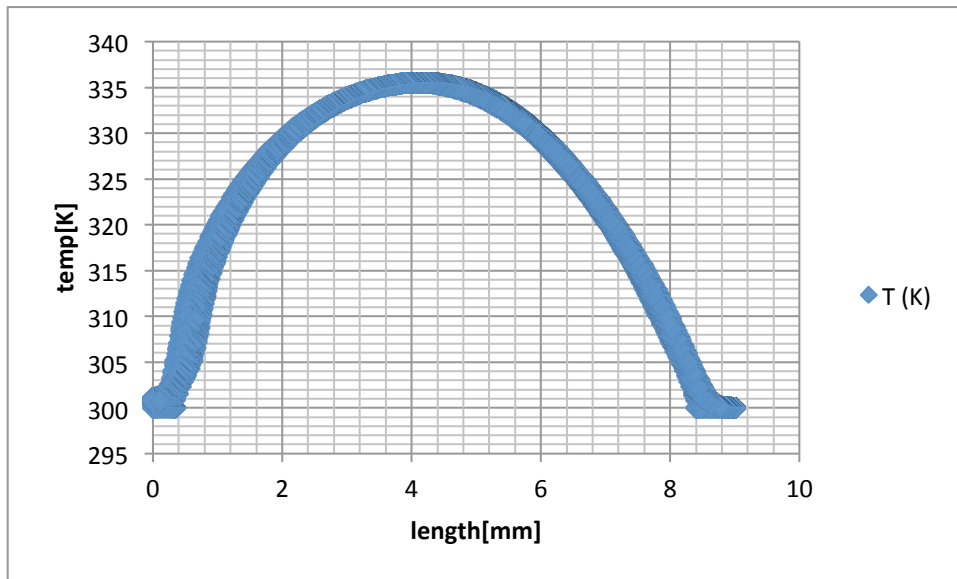


Figure 3.10 Temperature Distribution

From Comsol , we also get displacement and temperature distribution on wire as shown in Figure 3.9 and 3.10 which is in agreement with experimental results. Graphs show that maximum temperature occurs in the middle of the wire. In this sense, displacement is proportional with temperature distribution. This is another indication, showing that simulation is right [11].

Chapter 4

Cyclic Vibration Test

Repetitive prescribed displacement is applied to the first foot of the wire, and fatigue failure is detected by Wheatstone bridge. It is aimed to understand how the different wire geometries responses this test.

4.1 Experimental Set Up

As shown in Figure 4.1, shaker “Et-a26B-1” is utilized. It is an electric-mechanical transducer which provides controlled cyclic vibration.

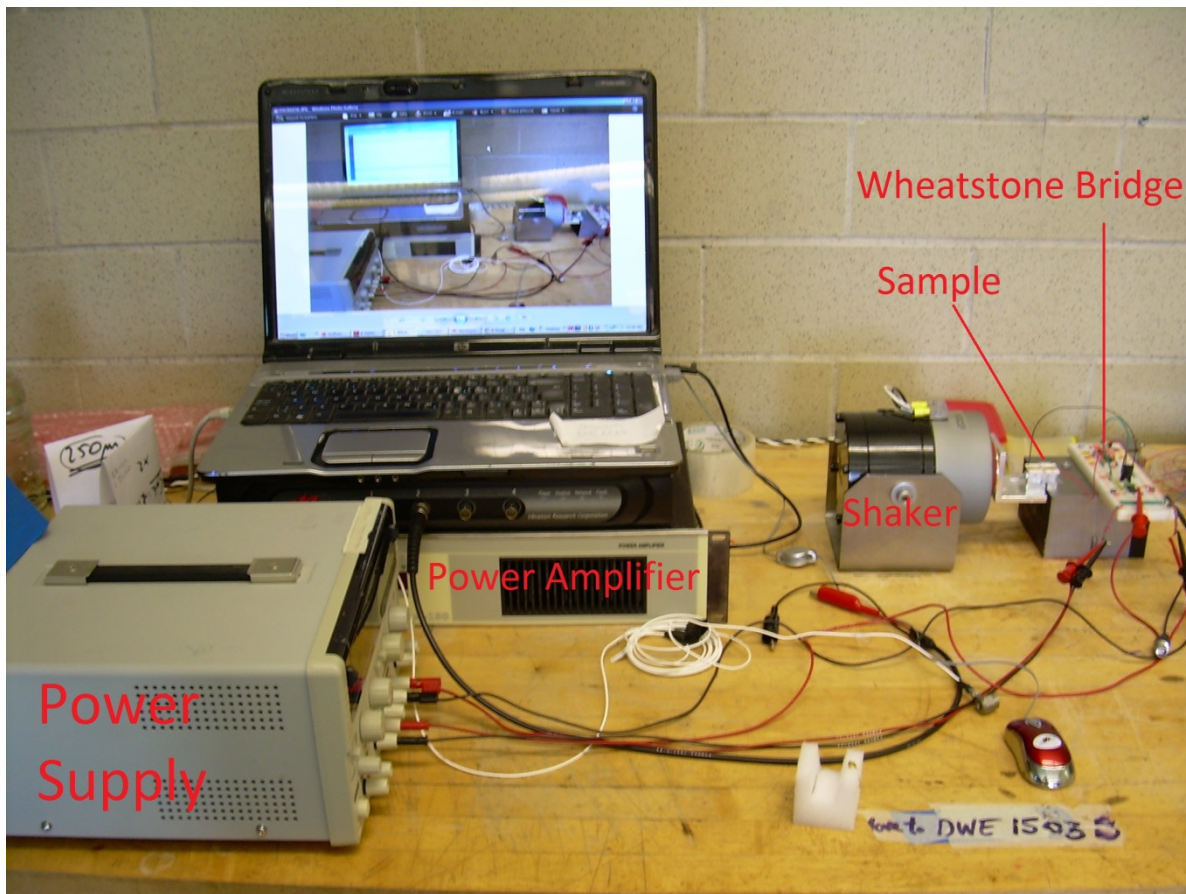


Figure 4.1 Vibration Experimental Setup

Wire bonds electrical resistance change with the effect of fractures and fatigue due to vibrations, so we decide to measure the wire electrical resistance over the experiment interval through a precise highly sensitive circuitry to detect fractures due to vibrations.

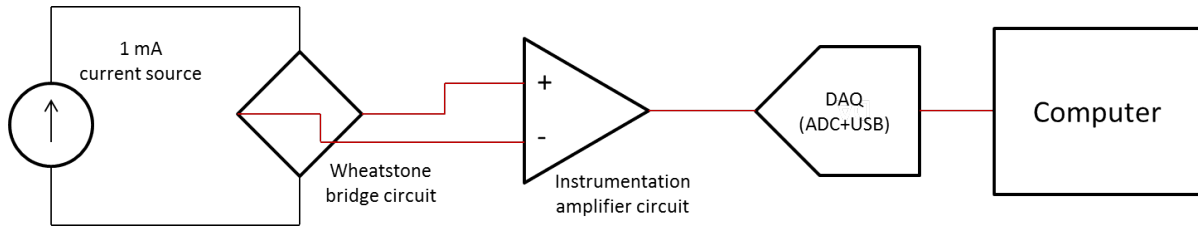


Figure 4.2 Test Circuit

The testing circuit block diagram and schematic shown in figures “a” and “b”, consists of a Wheatstone bridge circuit the wire bond is connected to one of its resistors ($R_w + \Delta R$) and its it supplied with a precision supply voltage and current of 1 mA to avoid any thermal effect on the wire bond due to current, then the output of the Wheatstone bridge circuit is amplified with the instrumentation amplifier, and the final stage the amplifier output is digitized and sent to computer through a data acquisition system for further analysis and monitoring.

As long as the wire bond is fine without any fractures due to fatigue the Wheatstone bridge will be balanced and the differential output voltage from it “ V_+ ” and “ V_- ” will be zero, once the wire bond starts to crack the value of resistance “ $R_w + \Delta R$ ” resulting in unbalancing the bridge circuit that will be seen as change in “ V_+ ” and “ V_- ”, however, the change in the output voltage is very small and unclear for monitoring and post analysis required so the output voltage is amplified with the “INA126” instrumentation amplifier, then the amplifier

output is supplied to the data acquisition system (Analog to Digital converter plus a computer interface like USB or ethernet) to be digitized and stored.

The current source circuit is used to supply the wheatstone bridge with a very small current of 1 mA to avoid the thermal effect of electric current on the wire bond cause it might interfere with the results and mislead the post analysis process.

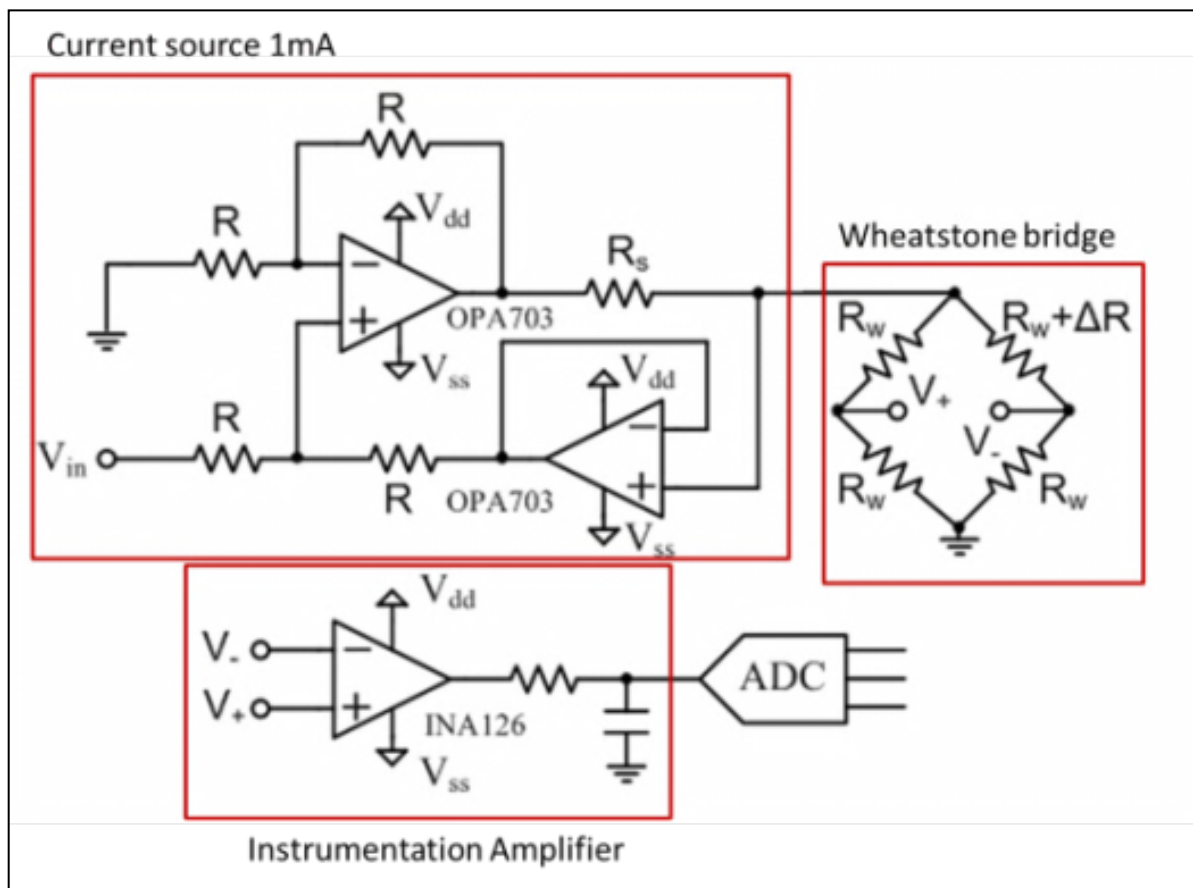


Figure 4.3 Test circuit schematic

4.2 Mathematical Model

The bonding wire is modeled using Euler-Bernoulli beam theory taking into consideration the initial curvature of bonding wires. We assume that the wire has a uniform circular cross-section with radius r , area A , and second moment of area I and loop height d . It is made of a homogeneous material with mass per unit length m , length L , and modulus of elasticity E . The bonding heels are assumed to be perfectly bonded to the silicon wafer.

In this analysis, we assume that the bonding wires are subject to in-plane support oscillations due to external mechanical vibrations. The partial differential equation describing the in-plane transverse vibrations due to an external axial force $\hat{P}(\hat{t})$ and an external lateral force

$\hat{F}(\hat{x}, \hat{t})$ is given by [16]

$$\rho A \frac{\partial^2 \hat{w}}{\partial \hat{t}^2} + \hat{c} \frac{\partial \hat{w}}{\partial \hat{t}} + EI \frac{\partial^4 \hat{w}}{\partial \hat{x}^4} + [\hat{P}_o + \hat{P}(\hat{t})] \left[\frac{\partial^2 \hat{w}}{\partial \hat{x}^2} + \frac{d^2 \hat{w}_o}{d \hat{x}^2} \right] \quad (1)$$

$$- \frac{EA}{2L} \left[\frac{\partial^2 \hat{w}}{\partial \hat{x}^2} + \frac{d^2 \hat{w}_o}{d \hat{x}^2} \right] \left[\int_0^L \left\{ \left(\frac{\partial \hat{w}}{\partial \hat{x}} \right)^2 + 2 \left(\frac{\partial \hat{w}}{\partial \hat{x}} \frac{d \hat{w}_o}{d \hat{x}} \right) \right\} d \hat{x} \right] = \hat{F}(\hat{x}, \hat{t})$$

subject to the boundary conditions

$$\hat{w}(0, \hat{t}) = 0, \quad \frac{\partial \hat{w}}{\partial \hat{x}}(0, \hat{t}) = 0 \quad \text{and} \quad \hat{w}(L, \hat{t}) = 0, \quad \frac{\partial \hat{w}}{\partial \hat{x}}(L, \hat{t}) = 0 \quad (2)$$

where \hat{P}_o is the residual axial force at the bond due to wire curvature, $\hat{P}(\hat{t})$ is an externally applied normal force, and $\hat{w}(\hat{x}, \hat{t})$ is the transverse deflections past the initial curvature shape of the wire.

Nondimensionalization provides a simpler form of the equations where the system parameters are lumped into few nondimensional groups. In this regard, we introduce the new variables

$$x = \frac{\hat{x}}{L}, w_0 = \frac{\hat{w}_0}{r}, \psi = \frac{\hat{\psi}}{r}, w = \frac{\hat{w}}{r} \text{ and } t = \frac{\hat{t}}{T} \quad (3)$$

where T is a time scale. Introducing these variables into Eq. (1) gives

$$\begin{aligned} & \frac{\partial^2 w}{\partial t^2} + c \frac{\partial w}{\partial t} + \frac{\partial^4 w}{\partial x^4} + \alpha_1 [\hat{P}_o + \hat{P}(\hat{t})] \left[\frac{\partial^2 w}{\partial x^2} + \frac{d^2 w_0}{dx^2} \right] \\ & - 2 \left[\frac{\partial^2 w}{\partial x^2} + \frac{d^2 w_0}{dx^2} \right] \int_0^1 \left\{ \left(\frac{\partial w}{\partial x} \right)^2 + 2 \left(\frac{\partial w}{\partial x} \frac{dw_0}{dx} \right) \right\} dx = \alpha_2 \hat{F}(\hat{x}, \hat{t}) \end{aligned} \quad (4)$$

and

$$w(0, t) = 0, \frac{\partial w}{\partial x}(0, t) = 0 \text{ and } w(1, t) = 0, \frac{\partial w}{\partial x}(1, t) = 0 \quad (5)$$

where

$$c = \frac{\hat{c} L^2}{\sqrt{\rho A E I}}, T = \sqrt{\frac{\rho A L^4}{E I}}, \alpha_1 = \frac{L^2}{E I}, \alpha_2 = \frac{L^4}{E I r} \quad (6)$$

The wire shape initially, $w_0(x)$, is approximated, respectively, by [16]

$$w_0(x) = \frac{1}{2}a(1 - \cos 2\pi x) \quad (7)$$

Moreover, c is the thermo-elastic damping coefficient. The externally applied mechanical axial force $\hat{P}(\hat{t})$ and transverse force $\hat{F}(\hat{x}, \hat{t})$ are assumed to be simple harmonic. The parameter a quantifies the rise of the wire at its midspan due its initial curvature.

To solve Eq. 4, we use a reduced-order modeling (ROM) scheme [17] where the in-plane response can be assumed as

$$w(x, t) = \sum_{i=1}^n u_i(t) \phi_i(x) \quad (8)$$

The suggested reduced-order model provides the advantage of reducing the order of the system, thus reducing the computational cost. On the other hand, since we are taking the effects of initial curvature and midplane stretching into account, the model is expected to efficiently capture the dynamics of vibrating bonding wires subject to thermal stresses and mechanical disturbances.

A first step in solving Eq. (4) is to find the wire mode shapes. To achieve this goal, we solve the linear, undamped, free vibration problem which is obtained by dropping the damping, forcing, and nonlinear terms of Eq. (4). The result is

$$\frac{\partial^2 w}{\partial t^2} + \frac{\partial^4 w}{\partial x^4} + N \frac{\partial^2 w}{\partial x^2} - 4 \frac{d^2 w_o}{dx^2} \int_0^1 \frac{\partial w}{\partial x} \frac{dw_o}{dx} dx = 0 \quad (9)$$

where $N = \alpha_1 P_o$ represents the residual stress within the wire before any external loading.

Solution of Eq. (9) is assumed in the form $w(x, t) = \phi(x) e^{-i\omega t}$. Sunstituting in Eq. (9) gives

$$\phi^{iv}(x) + N \phi''(x) - 4 w_o''(x) \int_0^1 \phi'(x) w_o'(x) dx = \omega^2 \phi(x) \quad (10)$$

which can be simplified to

$$\phi^{iv}(x) + N \phi''(x) - \omega^2 \phi(x) = 8 a^2 \pi^3 \cos(2\pi x) \int_0^1 \phi'(x) \sin(2\pi x) dx \quad (11)$$

The solution of Eq. (11) is composed of a homogenous part, $\phi_h(x)$ and a particular part,

$\phi_p(x)$. The homogeneous part of solution takes the form

$$\phi_h(x) = c_1 \sin(\beta_1 x) + c_2 \cos(\beta_1 x) + c_3 \sinh(\beta_2 x) + c_4 \cosh(\beta_2 x) \quad (12)$$

where

$$\beta_1 = \sqrt{-\frac{N}{2} + \sqrt{\frac{1}{4}N^2 + \omega^2}} \quad \text{and} \quad \beta_2 = \sqrt{\frac{N}{2} + \sqrt{\frac{1}{4}N^2 + \omega^2}} \quad (13)$$

In view of Eq. (11), the complimentary part of solution is assumed in the form

$\phi_p(x) = c_5 \cos(2\pi x)$. Thus we can write

$$\phi(x) = c_1 \sin(\beta_1 x) + c_2 \cos(\beta_1 x) + c_3 \sinh(\beta_2 x) + c_4 \cosh(\beta_2 x) + c_5 \cos(2\pi x) \quad (14)$$

Applying the boundary conditions given by Eq. (5) gives five equations in the constants c_i

and the parameters β_1 and β_2 which can then be solved for the natural frequencies and mode

shapes.

4.3 Experiment Results

	Wire (H/L) ,(AR)	Displacement	Number of Cycle to Failure
1	3/11 , (0.27)	39.4 um	142124
2	3/9 , (0.33)	31.45 um	467250
3	3/10 , (0.3)	35 um	221700
4	3.5/11, (0.318)	34 um	288754

Table 4 Vibration test Results

Tests are performed under 250 Hz. with different displacements between 31um to 39.4um.

Figure 4.4 shows the crack initiation point for wire. Circuit can detects wire cracking point which gives us chance to know failure time.

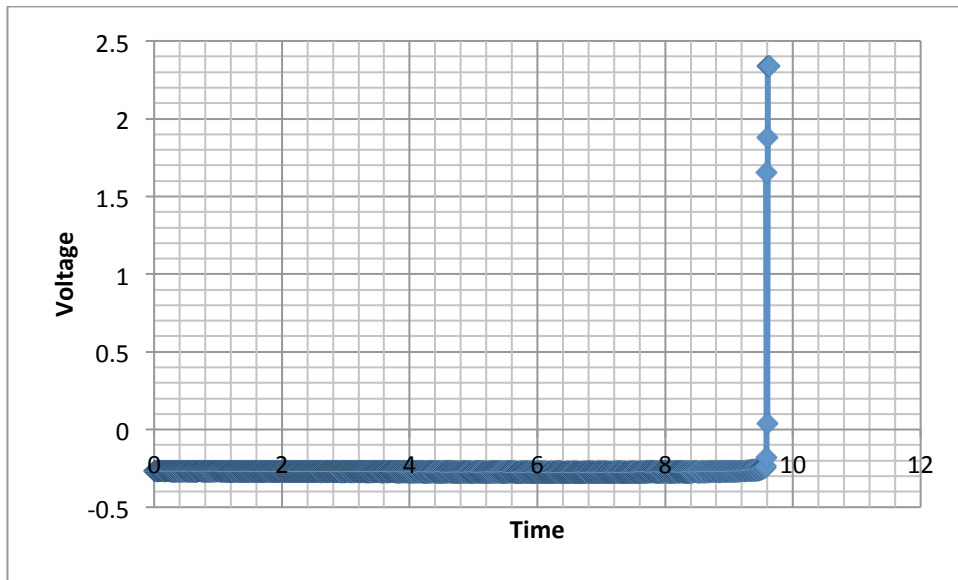


Figure 4.4 Failure Detection

Figure 4.5 shows SEM images of wire crack. It is cracked from heel as expected.

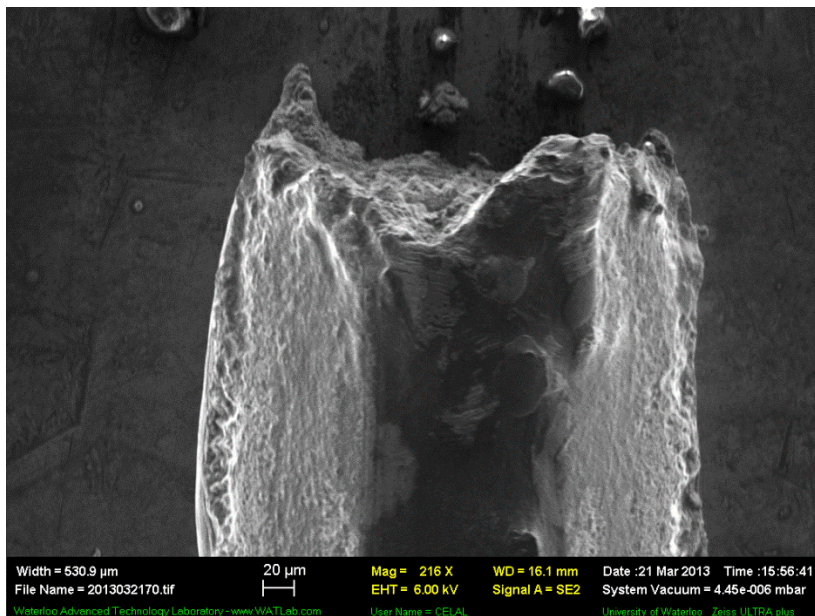


Figure 4.5 Heel Crack SEM Image

Chapter 5

Conclusion

Two test mechanisms are built and utilized. Joule Heating experiment shows the displacement and current relation. From this point of view, it is realized that wires have different displacement property depending on their geometry and material. Maximum displacements are observed for Al-H11 instead of CuCorAl and PowerCu. Therefore, simulations result is proved by experiment. It is also realized that wire AR (aspect ratio) has strong relation with displacement; higher AR means higher displacement.

Vibration test is succeeded and crack is caught using wheatstone bridge. SEM images prove heel crack failures due to the fatigue, as shown in literature.

A number of projects could be taken up ;

Further data collection to compare vibration and temperature cyclic test results. It would be interesting to find out temp. cyclic and vib. test relation. Vibration test can be considered for time saving.

Fatigue Prediction of different materials due to cyclic vibration could be investigated

Analytical Model can be improved adding Joule Heating effect on wire

Bibliography

[1] Tummala R., Fundamentals of Microsystems Packaging McGraw Hill, New York, 2001

[2] Harman G., Wire Bonding in Microelectronics: Materials, Processes, Reliability, and Yield, 2nd ed., McGraw Hill, New York, 1997

[3] Meyyappan, K. N., “Failure Prediction of Wire Bonds Due to the Flexure “-Marryland, 2004

[4] IGBT Modules , Infineon Company

[5] O. Schilling , M. Schäfer, K. Mainka, M. Thoben, F. Sauerland., “Power cycling testing and FE modelling focussed on Al wire bond fatigue in high power IGBT modules”, Microelectronics Reliability 52 (2012) 2347–2352

[6] Ramminger, S., Seliger, N., Wachutka, G., “Reliability Model for Al Wire Bonds subjected to Heel Crack Failures”, Microelectronics Reliability, Vol. 40, pp 1521-1525, 2000.

[7] M. Mermet-Guyennet, , X. Perpiñá, M. Piton,” Revisiting power cycling test for better life-time prediction in traction”, Volume 47, Issues 9–11, 2007

[8] Merkle, L., Kaden, T., Sonner, M., Gademann, A., Turki, J., Dresbach, C., Petzold, M. “Mechanical fatigue properties of heavy aluminium wire bonds for power applications” Proceedings - 2008 2nd Electronics Systemintegration Technology Conference

[9] Lefranc G, Weiss B, Klos C, Dick J, Khatibi G, Berg H.,”Aluminum bond-wire properties after 1 billion mechanical cycles”, Microelect Reliability 43 (2003)1833-1838. 003; 43:1833–8.

- [10] Volke, A., Hornkamp, M., IGBT Modules (Technologies , Driver and Application), 2010
- [11] Medjahed, H. , Vidal, P. , Noarede, B. “Thermo-mechanical stress of bonded wires used in high power modules with alternating and direct current modes”, Microelectronics Reliability
- [12] Medjahed, H., Vidal, P., Noarede, B “Comparison between electromagnetic and thermal stress induced by Direct Current flow in IGBT bond wires”, CIPS 2012, March, 6-8, 2012, Germany
- [13] Heraeus Brochure,”Power Cu, Large Diameter Copper Bonding Wire for Power Applications”
- [14] Heraeus Brochure,” Al-H11, Standard Aluminum Wire for Automotive and Power Applications”
- [15] "psv-400-scanning-vibrometer." vibration-sensors. 2013. Polytec,<http://www.polytec.com/us/products/vibration-sensors/scanning>
- [16] W. Lacarbonara, “A Theoretical and Experimental Investigation of Nonlinear Vibrations of Buckled Beams,” MS thesis, Virginia Tech, 1997.
- [17] M. Younis, E. Abdel-Rahman, and A. Nayfeh, “A Reduced-Order Model for Electrostatically Actuated Microbeam-Based MEMS,” Journal of Microelectromechanical Systems, Vol. 12, 672-680 (2003)
- [18] L'intérieur d'un module (bras de pont) IGBT 400 A / 600 V, technologie P.